

# A New Seismic Phase From Earthquakes Beneath the Japan Sea, Generated Near the Moho Discontinuity

journal or publication title	国立防災科学技術センター研究速報
number	78
page range	1-12
year	1988-11-17
URL	<a href="http://id.nii.ac.jp/1625/00002815/">http://id.nii.ac.jp/1625/00002815/</a>

## **A New Seismic Phase From Earthquakes Beneath the Japan Sea, Generated Near the Moho Discontinuity**

by

**Shoji Sekiguchi\***

*National Research Center for Disaster Prevention  
Science and Technology Agency  
Tsukuba, Ibaraki 305  
Japan*

### **Abstract**

A new seismic phase has been identified on seismograms at 12 stations in central Honshu, Japan from several earthquakes beneath the Japan Sea (denoted as X-phase). Analysis of the X-phase arrivals could provide information about the geometry and the location of laterally heterogeneous boundaries. The characteristics of the X-phase are: (1) the arrival time differences relative to initial *P* are 11 to 15 seconds; (2) the wave type is of *P* wave; (3) the apparent velocities are between 7.59 km/sec and 7.07 km/sec. It is inferred from these observations that the X-phase is generated near the Moho discontinuity and travels in the crust, multi-bouncing at the free surface and the Moho discontinuity. To generate the X-phase, lateral heterogeneity in the velocity near the Moho is needed. One possible interpretation is that there is a dipping interface across which the changes of *P* velocities of more than 5% occur at distance 1.1 to 2.3 degrees from the stations.

### **1. Introduction**

A new seismic phase was observed at seismic stations in central Honshu, Japan from several deep earthquakes beneath the Japan Sea. The characteristics of this phase and the interpretation of its generation in terms of lateral heterogeneity are described herein. This new seismic phase is called "X-phase".

### **2. The New Seismic Phase**

The X-phase is identified from deep earthquakes beneath the northern Japan Sea. Fig. 1 shows locations of the stations and the earthquakes which recorded and generated the X-phase, respectively. The origin times and the locations of these earthquakes are shown in Table 1. X-phase arrivals were looked for but not observed in seismograms

---

\* 2nd division seismic activity laboratory.

from other deep earthquakes that occurred in the subducting plate beneath the area south of Honshu, Okhotsk Sea or the central and eastern Japan Sea. The stations, where the X-phase was observed, are located in a narrow zone near the Japan Sea. The X-phase is not identified at stations far away from the epicenters.

Fig. 2 shows the waveforms of the vertical component of the X-phase. The arrival times of this phase are between 11 sec and 15 sec after the first *P* arrivals.

In order to specify the wave type of the X-phase and its apparent velocity, the particle motion observed at station KTJ was investigated. At this station, the distinct X-phase was observed and three-component seismograms are available. Fig. 3 shows examples of the three-component seismograms and the particle motions observed at station KTJ. The predominantly longitudinally polarized particle motions implies that the X-phase arrives at the station as a *P* wave.

To obtain the incident angle of the X-phase to the earth's surface, the free surface effect on the particle motion was removed. A  $V_p/V_s$  value of 1.69, determined for southwest Honshu (Ukawa and Fukao, 1971) was used. We obtained the corresponding incident angles of the X-phase as 46 to 51 degrees (Table 2). We also obtained the incident angles of the first *P* phase. To check the correction of the free surface effect, these incident angles were compared with those calculated by ray tracing. The agreement of each value was good (Table 2), therefore the correction for the free surface effects are considered reliable.

Fig. 4(c) shows a *P* wave velocity structure beneath station KTJ. The velocity of the surface layer is 5.5 km/sec. Using this value, we obtained an apparent velocity of the X-phase, 7.07km/sec to 7.59km/sec. This apparent velocity is smaller than the velocity, 7.8km/sec, found immediately beneath the Moho discontinuity (Aoki et al., 1972).

Table 1. Origin times and locations of the earthquakes used in this study.

No.	Y	M	D	H	M	S	N(°)	E(°)	h(km)	Mb
1	1977	09	09	02	35	02.0	42.88	131.43	530	4.8 I S C
2	1979	12	25	03	36	52.3	43.23	131.26	523	4.9 I S C
3	1981	10	05	04	28	13.1	42.82	131.31	531	4.7 I S C
4	1983	09	28	07	59	13.90	41.187	132.511	522.1	5.1 E D R
5	1983	09	28	08	04	47.60	41.170	132.455	513.1	5.1 E D R
6	1983	10	08	07	45	26.68	44.229	130.741	557.9	5.7 E D R
7	1984	04	15	07	34	12.09	42.926	131.085	538.0	5.0 E D R

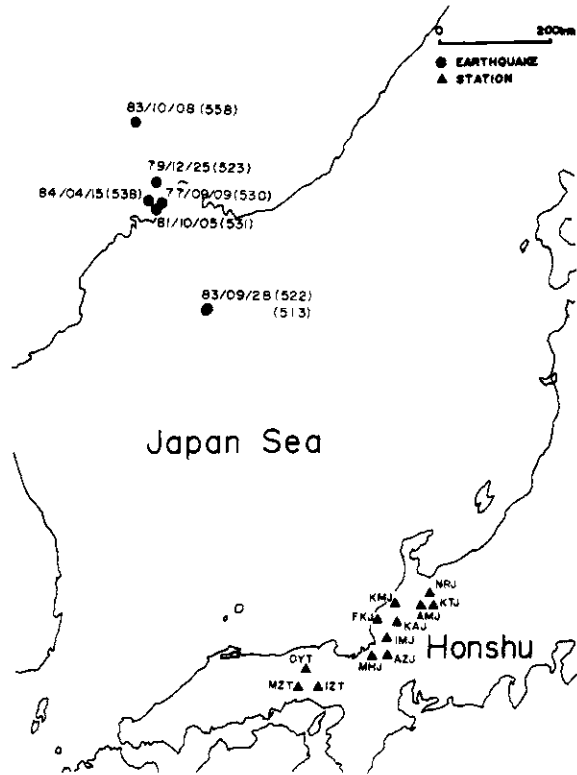


Figure 1. Stations and earthquakes. Triangles are the stations where the X-phase has been observed. Circles are the epicenters of the earthquakes, from which the X-phase is identified. Numbers in parentheses indicate the depths (km) of the earthquakes.

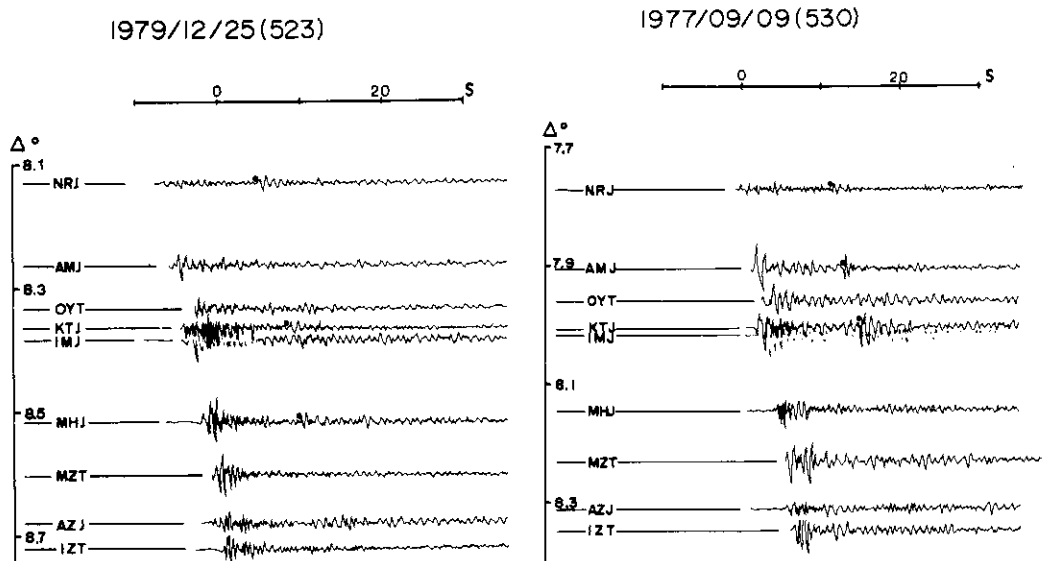


Figure 2. Waveforms of the X-phase. Dots indicate arrival times of the X-phase. The arrivals of this phase are between 11 and 15 seconds after the first P arrivals.

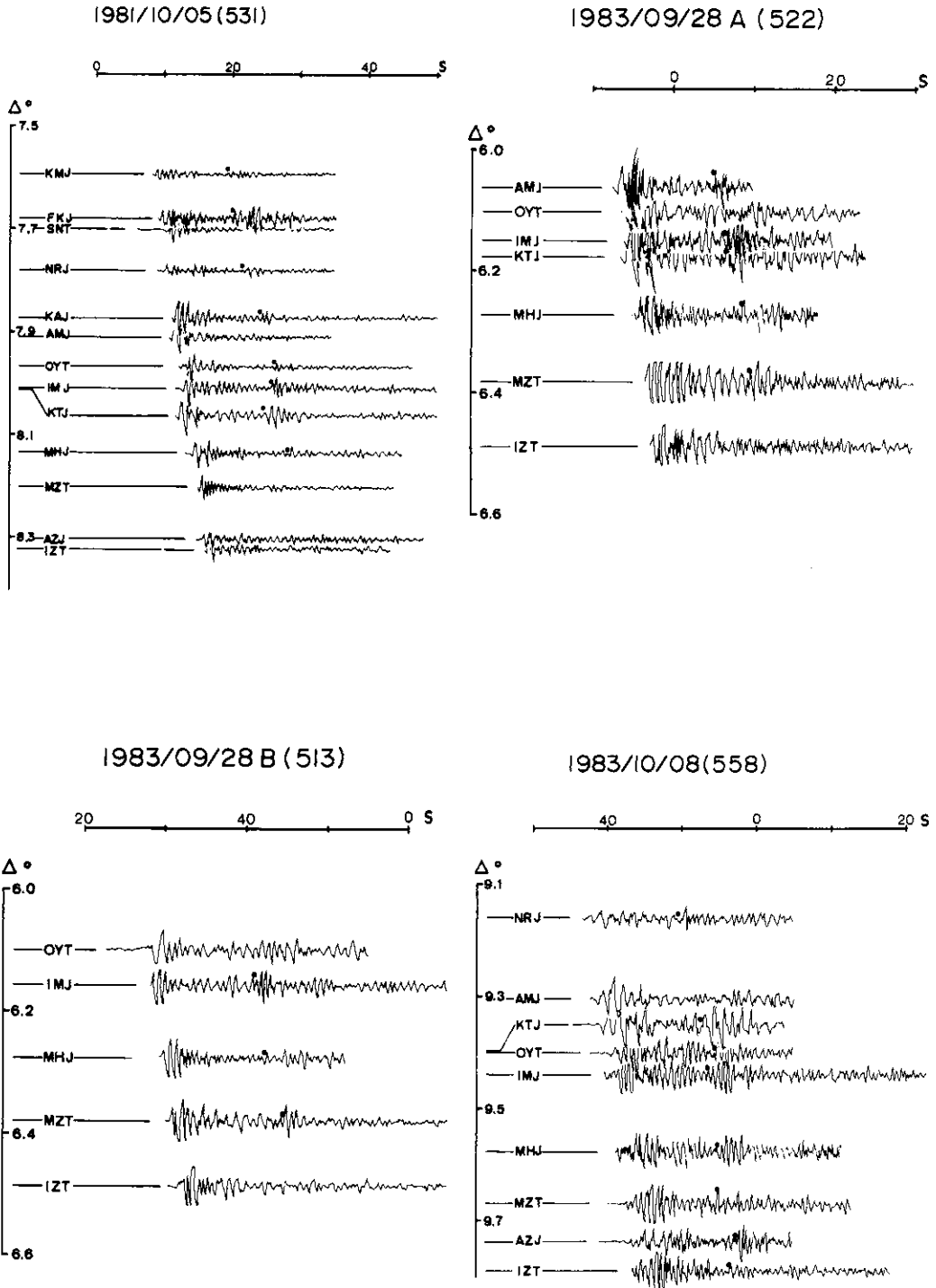


Figure 2. (Continued)

1984/04/15 (538)

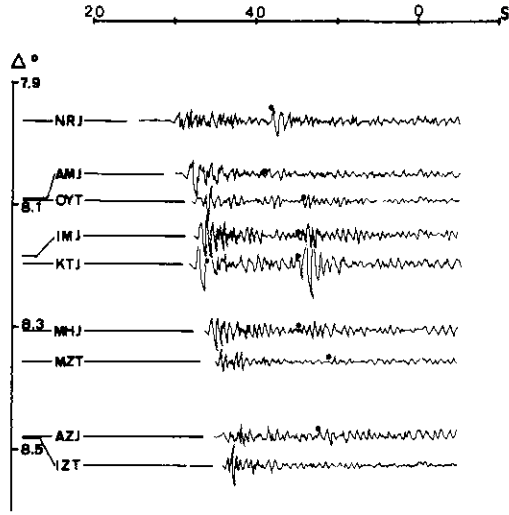


Figure 2. (Continued)

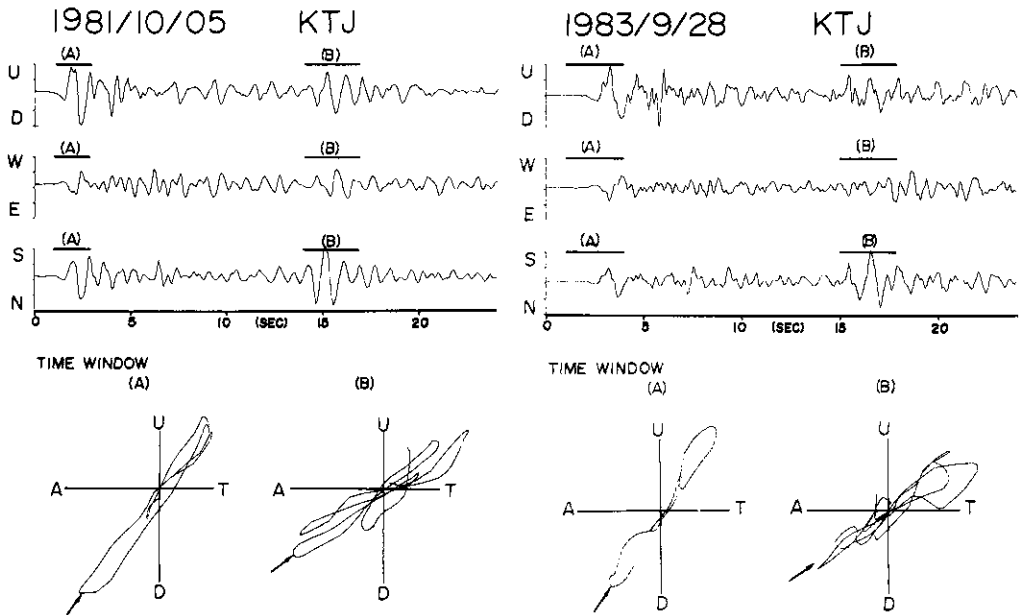


Figure 3. The three-component seismograms and the particle motions observed at station KTJ. Time window (A) and time window (B) include the initial phase and the X-phase, respectively. In the particle motion diagram, the abscissa indicates a radial component; "A" directs away from the station, "T" directs towards the station. The axis of the ordinate is vertical. (b) and (c) correspond to the NO. 4 and NO. 5 earthquakes in Table 1, respectively.

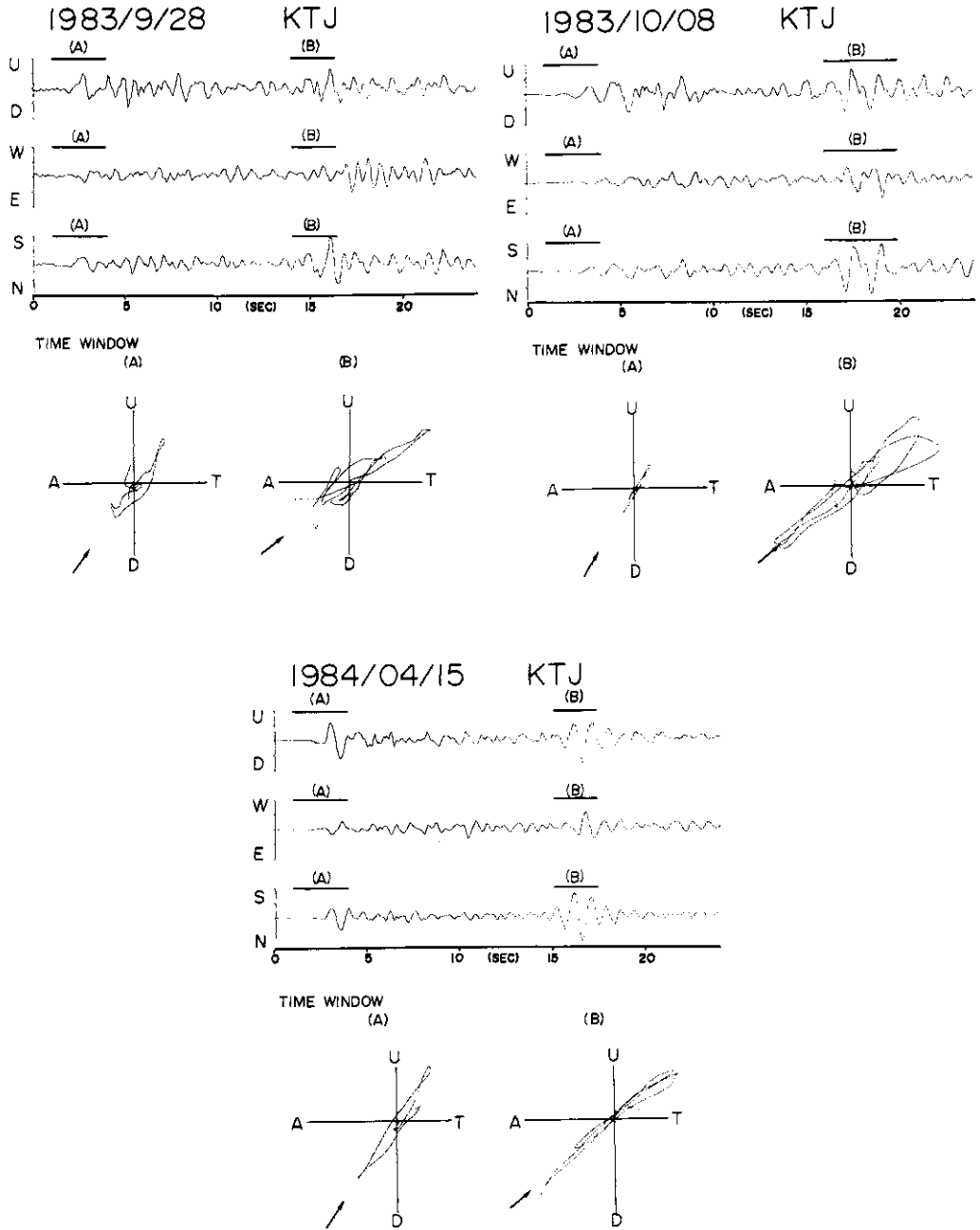


Figure 3. (Continued)

Table 2. Incident angles of the first *F* phases and the X-phases at KTJ.

No.	X-phase		first <i>P</i>		
	(Corr.)	(Obs.)	(Cal.)	(Corr.)	(Obs.)
3	50.5	54.3	30.0	32.1	36.7
4	51.1	54.8	28.3	29.2	33.6
5	47.9	52.1	28.6	30.4	34.9
6	47.8	52.0	29.9	26.8	30.9
7	46.5	50.8	29.9	29.9	34.3

'Corr.' means the incident angle with the correction of the free surface effect.

'Obs.' means the observed incident angle without the correction.

'Cal' means the calculated incident angle by the ray tracing.

### 3. Interpretation

In this section, possible mechanisms generating the X-phase will be investigated. Since the apparent velocity of the X-phase is smaller than any velocity in the mantle, generation of the X-phase should occur above the Moho discontinuity or where the velocity is smaller than the apparent velocity. If an *S* wave travels to the Moho discontinuity or an overlying discontinuity and converts to the X-phase, then the arrival time difference from the *P* to X phases would become significantly longer than those observed. This provides strong evidence that the X-phase is converted from a *P* wave which has traveled throughout the path from the seismic source to the conversion point. In the following part of this paper, any phase conversions such as *S* to *P*, before the ray arrives near the Moho plane, are not considered.

It is supposed that the X-phase is generated at the Moho discontinuity and propagates in the crust as a *P* wave in order to specify the distance of the location where the X-phase is generated. Ray paths of the X-phase are calculated backwards from the station, varying an incident angle to the station from 45 to 55 degrees. An incident angle slightly larger than the observed one is permitted for the calculation. The reason is that, in the ray tracing, the velocity structure with the layers of the thickness thinner than the actual thickness beneath the seismic station were used, as shown later. As a result, a slightly larger incident angle is required to satisfy the observed travel time differences of the *P* to X-phase. If the velocity structure with lateral heterogeneity is used in the ray tracing, the incident angle will be within the observed angles. The ray paths forward from the seismic source are also calculated. Then the two rays at the Moho discontinuity are connected to satisfy the observed *P*-to-X time. The incident angle is allowed to increase at the Moho discontinuity when the ray of the X-phase passes through there from the mantle.

Figs. 4(b) and (c) show velocity models for the crust beneath the northernmost point of Fig. 4(a) (open triangle) and beneath station KTJ (solid triangle), respectively. This velocity structure is the laterally homogeneous layered structure. Different velocity structures of the crust are used for the initial phase and the X-phase. For the initial phase, the velocity structure shown in Fig. 4(c) is used. For the X-phase, a crustal structure of the surface layer beneath KTJ and of the second and the third layers are used as shown in Fig. 4 (b), because X-phase travels in the crust in the north of the station KTJ. The Jeffreys-Bullen's velocity structure is used for below the Moho discontinuity.



The calculations show that two kinds of ray paths are possible to satisfy the observed *P*-to *X* arrival time difference (Fig. 5(a)). One ray reflects twice at the free surface and twice at the Moho discontinuity (case A). The other ray reflects once at each interface (case B).

In this way, the ray paths from all the sources to the stations are calculated and the locations where the *X*-phase crosses the Moho discontinuity are specified. Fig. 6(a) is a plot of the crossing points for the ray paths reflected twice at each boundary (case A). Open circles indicate the crossing points. The distances to the crossing points from the stations are 1.1 to 1.9 degrees. Fig. 6(b) shows a similar result for the ray path reflected once at each boundary (case B). The distances are 1.5 to 2.3 degrees.

As shown in Fig. 5(a), the incident angle of the two ray paths increase when the rays pass across the Moho discontinuity. However, the incident angle does not increase when the ray propagates in a laterally homogeneous medium. Thus, we believe that a laterally inhomogeneous structure is needed. One simple but likely velocity structure is suggested in Fig. 5(b): a higher velocity layer adjoins a lower velocity layer with a dipping interface resulting in increases of incident angles of the *X*-phase. This interface can exist either below the Moho discontinuity or within the crust. However, no data is available at present to determine its depth more precisely. Other possibilities can not be excluded at this time. There might be other velocity structures that can explain the increase of incident angles of this phase.

Finally, it is necessary to explain the amplitude of the *X*-phase relative to the first *P* phase. It is assumed that each phase impinges against the Moho discontinuity as a plane wave and has the same unit amplitude. Reflection-transmission coefficients at the interfaces are only considered in order to estimate the amplitudes. As an apparent velocity of the initial *P* phase, the observed one is taken, which corresponds to the incident angle of 30 degrees at the station (Table 2). In this way, it is found that the amplitude of the first *P* phase is 1.14. Next, the amplitude of the *X*-phase is estimated. As a first step, the case where the *X*-phase passes through the heterogeneous velocity structure, i.e., travels through the dipping interface and the Moho plane but does not reach the next interface in the crust, is considered. The dipping interface is assumed to exist beneath the Moho discontinuity. The dip angle of the interface is adjusted to satisfy the increase of the incident angle of the *X*-phase. The high velocity region of 7.8km/sec and the low velocity regions of 20% (6.24km/sec), 15% (6.63km/sec), or 10% (7.02km/sec) smaller than the high velocity are considered. The apparent velocity of the initial *P* wave is considered to be that of the *X*-phase impinging against the dipping interface. This apparent velocity corresponds to 45 degrees in the incident angle there, and this value is used in the estimation of the amplitude. As a next step, consideration is given to the case where the ray, after leaving the Moho plane, travels through the interfaces within the crust and reaches the station. The two kinds of ray paths, denoted by cases A and B previously, are considered. The ray element, numbered as 1 in Fig. 5(a), travels within the crustal structure shown in Fig. 4(c). The ray element, numbered as 2 in Fig. 5(a), travels within the crustal structure shown in Fig. 4(b). As an apparent velocity of the *X*-phase in the crust, either of the two apparent velocities which corresponds to the lower or upper limit of the observed incident angles of the *X*-phase at the free surface (45 or 50 degrees) are taken. These incident angles are used in the estimation. Table 3(a) summarizes the results of the dip angles and the products of the transmission coefficients in the first step. Table 3(b) shows the results of the products of the transmission-reflection coefficients in the second step. The amplitudes of the *X*-phase do not diminish so much in the second step, since the wide angle reflection occurs

at the Moho discontinuity. Amplitude of the X-phase at the station is obtained by multiplying each result with the same incident angle of the X-phase. The maximum amplitude is 0.43, obtained from case A at the incident angle 45 degrees. Some observed maximum amplitudes of the X-phase are as large as the first *P* phase amplitudes. The estimated maximum amplitude of the X-phase is about one third of the estimated amplitude of the first *P* wave. Therefore, the estimated amplitudes will be consistent with the observed ones. If the low velocity of only 5% smaller than the high velocity is taken, any dipping angles of the interface can not be adjusted to satisfy the increases of the incident angle of the X-phase. Therefore, a change of the *P* wave velocity of more than 5% across the dipping interface is needed.

The situation, where the ray of the X-phase always travels as a *P* wave within the crust, has been considered. It has been noted that by using the same consideration about the amplitude, when the X-phase goes through some wave conversions within the crust all of the amplitudes are smaller than the maximum amplitude of the X-phase with no wave conversion. Therefore, the X-phase without any wave conversion is most preferable in explaining the amplitude of the observed X-phase. The X-phase with wave conversions, however, might contribute the amplitude of the later part of the X-phase.

It was supposed that in the amplitude estimation the dipping interface, separating the high velocity region and the low velocity region, exists beneath the Moho discontinuity. There is no reason to exclude the possibility that the dipping interface might exist within the crust.

It was previously mentioned that the X-phase is associated with only the earthquakes beneath the Japan Sea. This implies that the proposed inclined velocity structure does not exist where the rays from the other earthquakes cross the Moho discontinuity. The X-phase is identified at the stations in a narrow zone along the coast of the Japan Sea. This phenomena can be explained if the proposed velocity structure is limited to a certain depth.

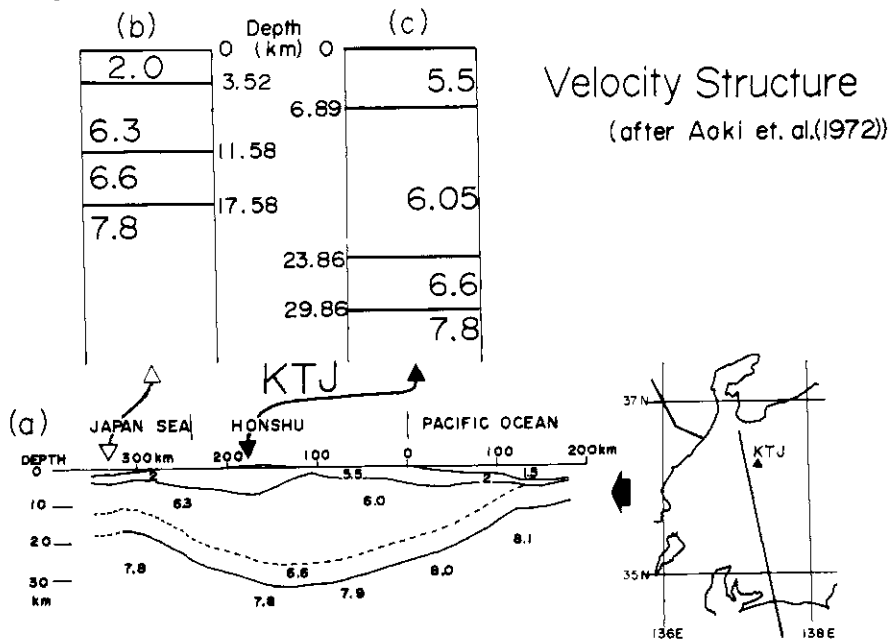


Figure 4. (a) P wave velocity structure near the stations (after Aoki et al. (1972)). (b) P wave velocity structure beneath the northernmost point of (a). (c) P wave velocity structure beneath station KTJ.

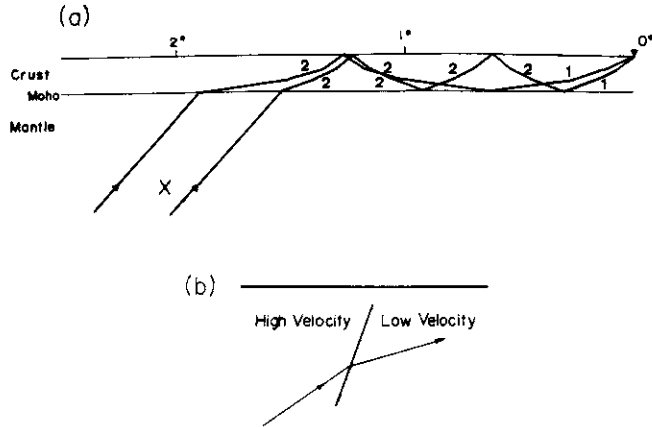


Figure 5. (a) Two possible ray paths, which satisfy the observed P to the X arrival time difference. One ray is reflected twice at the free surface and twice at the Moho discontinuity (case A). The other ray reflects once at each of the discontinuities (case B). The ray elements, numbered as 1 and 2, travel within the crustal structures shown in Fig. 4 (c) and (b), respectively. (b) A simple and likely velocity model which can generate the X-phase.

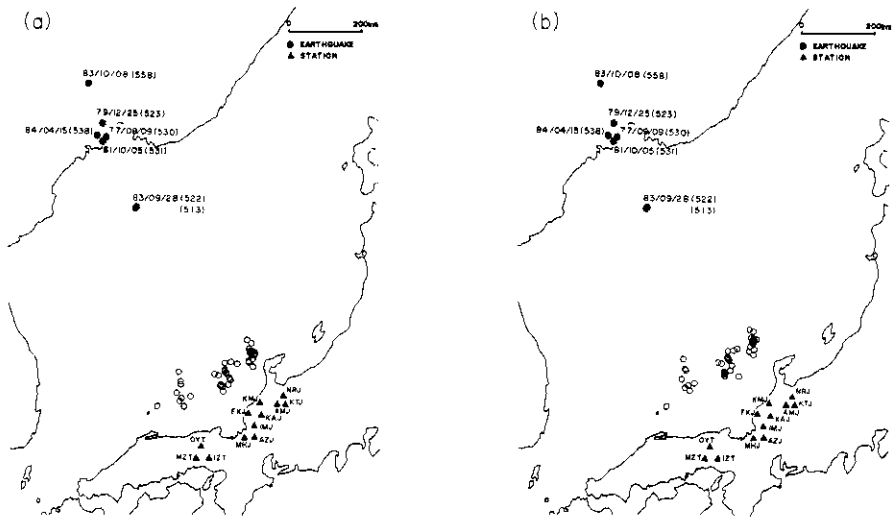


Figure 6. The locations of the ray crossing point of the X-phase at the Moho discontinuity (open circles). (a) denotes for the ray path reflected twice at each boundary (case A). (b) denotes for the ray path reflected once at each boundary (case B).

#### 4. Conclusion

In summary, the characteristics of the X-phase are as follows:

- (1) arrival time differences of *P*-to-X phase are 11 to 15 seconds;
- (2) X-phase is of *P* wave;
- (3) apparent velocities of the X-phase are between 7.59 km/sec and 7.07km/sec.

It is inferred from these observations that the X-phase travels to the Moho discontinuity as a *P* wave. The X-phase is generated near the Moho discontinuity with specific lateral heterogeneous velocity structures. After the reflections at the free surface and the Moho discontinuity, it arrives at the observational stations as a *P* wave. One of the specific velocity structures is that of a high velocity layer and a low velocity layer adjoined at a dipping interface.

With some constraints on the heterogeneous velocity structures, it can be inferred that the dipping interface exists at distances of 1.1 to 2.3 degrees. The change of *P* velocity is more than 5%. From a simple estimation of the amplitudes, it is found that the observed amplitude of the X-phase can be explained in this inferred velocity model and the X-phase with no wave conversion in the crust is most preferable in explaining the amplitude.

Table 3. Products of transmission-reflection coefficients  
(a) for the rays going through the heterogeneous region

incident angle <sup>(1)</sup> (degree)	low velocity <sup>(2)</sup> (km/sec)	dip angle <sup>(3)</sup> (degree)	products
45	6.24	-82	1.12
45	6.63	73	0.93
45	7.02	38	0.46
50	6.24	77	1.04
50	6.63	56	0.59
50	7.02	no solution	

(b) for the rays in the crust

incident angle <sup>(1)</sup> (degree)	case <sup>(4)</sup>	product
45	B	0.38
45	A	0.15
50	B	0.31
50	A	0.11

- (1) The incident angle of the X-phase impinging against the inclined interface.
- (2) The velocity for the lower velocity side in Fig. 5(b).
- (3) The dip angle of the inclined interface in Fig. 5(b), where the angle is measured from horizontal to downward directions and the positive and negative values of the angle mean that the interface dips to the seismic source and the station, respectively.
- (4) The case of the ray paths of the X-phase in Fig. 5(b) (see the text or the figure caption for the meaning of A and B).

## Acknowledgements

I wish to thank Masataka Ando for helpful discussions. I am grateful to the staff of the seismological observatories of Hokkaido, Tokyo, Nagoya, Kochi and Kyoto universities for permitting the use of their seismograms.

## References

Aoki, H., T. Tada, Y. Sasaki, T. Ooida, I. Muramatsu, H. Shimamura, and I. Furuya (1972): Crustal structure in the profile across central Japan as derived from explosion seismic observations. *J. Phy. Earth*, 20, 197-223.

Ukawa, M. and Y. Fukao (1981): Poisson's ratios of the upper and lower crust and the sub-Moho mantle beneath central Honshu, Japan. *Tectonophysics*, 77, 233-256.  
(manuscript received September 6, 1988)

## モホ不連続面近傍で発生した日本海下の地震による新地震波フェイズ

関口 渉次\*

国立防災科学技術センター

日本海下のいくつかの深発地震に対し、日本の本州中部の微小地震観測点に於いて、新しい地震波相が見つかった(以下これをX相と呼ぶ)。X相の到着時刻を解析することにより、横方向に変化する境界の形と位置に関する情報が得られた。X相の特徴としては、(1) P波に対して相対的な到着時刻が11秒から15秒になる、(2) 縦波である、(3) 見かけ速度は7.59 km/secから7.07km/secの間である、という点があげられる。これらの観測事実から、X相はモホ不連続面附近で発生し地殻内をモホ面と地表面で多重反射しながら伝わった、と推察される。X相を生成するためには、モホ面附近に速度の不均質が必要とされる。ひとつの可能な解釈として、観測点から1.1度から2.3度の距離のところに5%以上P波速度が変化する傾いた境界面がある、というモデルが考えられる。